EXPERIMENTALLY VALIDATED COUPLED MODELLING OF THE HEAT TRANSFER PROCESSES OF ELECTROMAGNETICALLY DRIVEN FLOW WITHIN A COLD-CRUCIBLE INDUCTION FURNACE

Bulinski P., Smolka J.*, Golak S., Przylucki R., Palacz M., Siwiec G., Lipart J., Blacha L.
*Author for correspondence
Institute of Thermal Technology,
Silesian University of Technology,
44-100 Gliwice,
Poland,
E-mail: jacek.smolka@polsl.pl

ABSTRACT

This paper presents a coupled numerical study of the thermal processes that occur in the vacuum induction furnace with a cold crucible. In this furnace type, the high quality metals like titanium are thermally processed. The perspective aim of this work is to improve crucible structure to reduce the skull volume on the basis of the validated numerical model. In the developed code, the two-way coupling of the electromagnetic and thermal phenomena is employed to mainly predict the shape and temperature of the melt free surface. Both these parameters were measured using contactless methods with infrared and high-speed cameras. Moreover, the shape and mass of the skull was also predicted and compared with the experimental data. The numerical simulations were performed for a repeating part of the full 3-D domain for three different portions of the titanium charge. In the coupling transient procedure, the electromagnetic submodel produced a field of power losses generated within the molten metal space, while the thermal model was responsible to generate the free surface shape. The data transfer after each time step was performed from the initial flat free surface until the monitored data became constant as observed during the tests in the lab. The results showed that compared shape and the temperature were predicted with a quite satisfactory accuracy.

INTRODUCTION

Cold crucible induction furnaces are the melting devices designed to produce metals and alloys of the highest quality in terms of purity. This product quality is achieved due to the limited contact of the metal with the crucible. As a result, the this kind of induction furnace is characterised by the ability of removing both volatile impurities and gases dissolved in the melt. On the other hand, the cold crucible furnace has a relatively low heating efficiency when compared to other induction furnaces. This is a result of both low electrical efficiency of this unit and a charge heat dissipation through intensively cooled crucible walls.

An investigation of the induction heating within a cold crucible of an induction furnace was considered in a previous study of Yang [1]. The authors developed a 2-D finite element model to obtain the thermal characteristics of three metals. The proposed mathematical formulation defined the coupling between the temperature and electromagnetic fields in a solid charge. To validate the numerical model, five thermocouples were inserted into the crucible charge at specified heights. The proposed model produced results that were in good agreement with the experimental test performed for three metals.

NOMENCLATURE

$\boldsymbol{A}$	[Vs/m]	Magnetic vector potential
$\boldsymbol{F}$	[N]	Lorentz force
$\boldsymbol{g}$	[m/s^2]	Gravitational acceleration vector
$\boldsymbol{J}$	[A/m^2]	Current density source
J	[m^2/s]	Diffusion flux
P	[W]	Supply active power
P	[Pa]	Pressure
t	[s]	Time
$\boldsymbol{V}$	[V]	Electric scalar potential
V	[m^3]	Volume of the charge
$\boldsymbol{v}$	[m/s]	Velocity vector
Y		Mass fraction

Special characters

η		Efficiency
μ	[H/m]	Magnetic permeability
μ	[kg/m/s^2]	Dynamic viscosity
σ	[S/m]	Magnetic conductivity
ω	[rad/s]	Angular frequency
ρ	[kg/m^3]	Density

Subscripts

a	Active
e	Eddy current
$EMAG$	Electromagnetic
ST	Surface tension
s	Source
q	Phase

The recent study of Hadad et al. [2] presented a novel approach for predicting the temperature distribution within the vacuum inductive heating process. They performed simulations and experiments for a stepped diameter crucible with a secondary heating coil. The numerical results were validated against measurement data that were recorded by means of thermocouples located inside a region of the large diameter. The numerical results showed good correlation with the experimental results.

Most comprehensive coupling of the flow, temperature and electromagnetic fields was presented by Bojarevics et al. [3]. The authors developed a numerical model of an induction skull melting furnace to simulate the behaviour of four materials. To track the shape of the free surface, a surface spectral-collocation mesh was applied. The validation process was performed in a few ways: the qualitative shape of the free surface, the meniscus height, the charge and the cooling water temperature and, finally, the heat losses. The authors reported very accurate results, proving that the application of 2-D space modelling is adequate for such problems.

As discussed above, numerical computations of induction furnaces are mainly focused on free surface flow [4] and induction heating efficiency [5] and impurities removal process [6]. To successfully describe these processes inside the furnace, it is necessary to develop a two-way coupling between the computational fluid dynamics (CFD) and electromagnetic (EMAG) solutions. In previous numerical work of this research team [7], such a coupling procedure was developed and then examined for different operating conditions [8]. The latest investigation [9] showed that the proposed mathematical model and coupling procedure despite its simplicity yields reasonable accuracy in terms of the heat transfer and free surface prediction.

Hence the main aim of the present study was to numerically simulate the thermal and the flow processes that occur in the vacuum induction furnace with a cold crucible. For this reason, the high quality metal, i.e. titanium was thermally processed. Then the numerical simulations of the impurities removal process within the considered induction furnace were performed. In this case, the considered charge was the copper-lead alloy with the initial lead mass fraction of 2%. The coupled computations were performed for different input power of the inductor. The results showed a strong influence of the inductor power on the free surface area and, therefore, on purification process intensity.

COMPUTATIONAL DOMAIN

The investigated object was the real vacuum induction furnace produced by Seco-Warwick and installed at the Institute of Metal Technology of the Silesian University of Technology, Katowice, Poland. To reach a high vacuum, this unit is equipped with a system of three vacuum pumps that can provide the minimum pressure of 10 mPa. The maximum inductor power of this unit is of 75 kW.

The developed model was formulated to couple the CFD and EMAG solutions. Therefore, separate geometrical models were generated. The scheme of both models is presented in Figure 1. As indicated in this figure, the coupled model included the charge, crucible, air above the charge and the inductor. In the case of the EMAG model, the air outside the crucible was a part of the geometrical domain. The presented geometry is a single segment that represents a repeating fragment of the whole crucible.

The mesh in the EMAG domain consisted of TET elements, while HEX elements were used to compose the grid for the CFD model. The former mesh included 25 thousand elements, while the latter included 100 thousand elements.

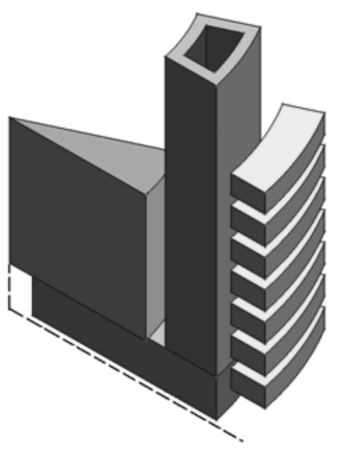

Figure 1 Scheme of the coupled model domain for the cool crucible

NUMERICAL COUPLED MODEL

The 3-D EMAG model of the cold crucible was developed determine the electromagnetic field. As a result, the electromagnetic force invoked by the inductor and the Joule heat generated in the charge were computed. In the uncoupled approach, it was assumed that the charge is in a solid state. In consequence, the problem of a free surface dynamics does not occur [10,11]. Then in the coupled procedure, the varying charge shape was considered in the EMAG model. The computations were performed using the open source code GetDP. This program using the finite element method enables to solve any system of partial differential equations.

The harmonic model of the electromagnetic field was based on formulation using the magnetic vector potential approach:

$$\nabla \times \left(\frac{1}{\mu} \nabla \times \underline{\mathbf{A}} \right) = \underline{\mathbf{J}}_{\mathrm{s}} + \underline{\mathbf{J}}_{\mathrm{e}} \tag{1}$$

The eddy currents density is solved based on the following equation:

$$\underline{\mathbf{J}}_{\mathrm{e}} = -\sigma \left(\mathrm{j}\omega \underline{\mathbf{A}} + \nabla \underline{\mathbf{V}} \right) \tag{2}$$

The second component taking into account in the AV formulation is the current continuity equation, i.e. the Gauss law for the electric field after transformation:

$$\nabla \cdot \underline{\mathbf{J}}_{\mathrm{e}} = 0 \tag{3}$$

Those equations were supplemented with the following material properties of the charge and crucible: magnetic permeability of all model components of $12.56 \cdot 10^{-7}$ H/m, electric conductivity of titanium charge and copper crucible of $2.4 \cdot 10^{6}$ S/m and $5.5 \cdot 10^{7}$ S/m, respectively. Then the periodicity boundary conditions were applied to the vertical sides of the computation domain. In addition, the boundary condition of the zero magnetic potential was defined on the outer surfaces of the EMAG model.

On the basis of solution of the above equations, the Joule heat was determined and then transferred to the CFD model:

$$q_{VJ} = \frac{\left|\underline{\mathbf{J}}_{\mathbf{e}}\right|^2}{\sigma} \tag{4}$$

The electrical efficiency of the cold crucible was defined as:

$$\eta = \frac{\int_V q_{VJ}\,\mathrm{d}V}{P_a} \cdot 100\% \tag{5}$$

The CFD submodel was defined in Ansys Fluent. To predict free surface shape, the mass and momentum conservation equations were solved. These equations for the considered geometry can be expressed as follows:

$$\frac{\partial}{\partial t}\left(\alpha_q \rho_q\right) + \nabla\left(\alpha_q \rho_q \mathbf{v}\right) = 0 \tag{6}$$

$$\frac{\partial}{\partial t}\left(\rho \mathbf{v}\right) + \nabla\left(\rho \mathbf{v}\mathbf{v}\right) = -\nabla p + \mu \nabla^2 \mathbf{v} + \rho \mathbf{g} + \mathbf{F}_{EMAG} + \mathbf{F}_{ST} \tag{7}$$

Furthermore, to simulate the impurities removal from the induction furnace, an additional conservation equation for the species mass fraction was solved:

$$\frac{\partial}{\partial t}\left(\rho Y_i\right) + \nabla \cdot \left(\rho \mathbf{v} Y_i\right) = -\nabla \cdot \mathbf{J}_i \tag{8}$$

A flow within an induction furnace crucible is strongly turbulent due to the intensive electromagnetic mixing. Therefore, it was necessary to employ a turbulence model, i.e. *k-ω*. The defined set of differential equations was completed by material properties. Those of the molten titanium were as follows: density 4130 kg/m^3 and dynamic viscosity 0.00045 kg/m/s, while the copper-lead alloy properties were density 8000 kg/m^3 and dynamic viscosity 0.00375 kg/m/s. To simplify model, the air was examined as gas with the constant value of the density and dynamic viscosity of 1.225 kg/m^3 and $1.7894 \cdot 10^{-5}$ kg/m/s, respectively. The mass diffusivity was assumed to be constant value of $2 \cdot 10^{-8}$ m^2/s. To model lead transport through the free surface, the overall mass transport coefficient of $6 \cdot 10^{-5}$ m/s was determined according to the experiment data.

COUPLING PROCEDURE

The in-house two-way coupling code was implemented by means of the User Defined Functions (UDF) of the ANSYS Fluent package. This code was used to transfer the information regarding the computational domain shape and to launch the EMAG solver. The EMAG computations produced two output fields, i.e. the Lorentz force components and the Joule heat distributions. Then, this information was imported to the CFD submodel as the source terms for the momentum and energy transport equations.

Due to high instability of the process and rapid free surface changes, the computations were performed in an unsteady state using short time steps. To maintain a low Courant number, which was required by the explicit multiphase solver, the time step of 0.0001 s was applied. Such a small time step resulted in a long computing time, especially due to the poor convergence of the temperature field. To avoid this problem, it was decided to limit the coupled multiphase simulations to the moment when the molten metal geometry had converged. Then, the temperature field was computed in the decoupled thermal model. The molten metal shape was maintained in one position, and the free surface became a new external boundary condition. This approach enabled increasing the time step to 1 s.

RESULTS DISCUSSION

To qualitatively verify the numerical model, the Joule heat and the Lorentz force fields and their influence on the flow and thermal fields were examined. The largest concentration of the Lorentz force vectors occurred in the near-wall regions of the charge. The maximum values of the electromagnetic force were directed radially towards the axis of the charge forming the meniscus and several vortices. The first group of eddies appeared in the meniscus region, while the second group was located in the lower area of the molten metal. The latter group was significantly more intensive, while the former encompassed a larger area. It is worth noting that the groups of vortices swirled in opposite directions. The highest noticed velocity was 0.75 m/s, and it was located near the bottom crucible wall.

To perform the model validation on the basis of the meniscus shape, high-speed camera experiments were carried out. The obtained numerical results and experimental data of the molten metal free surface for three power values of the inductor were presented in Figure 2. In particular, the numerical meniscus shape was compared with the experimental maximum meniscus height and its marked standard deviation. It has to be noted that the real heating/melting process in this induction furnace was highly unstable. In consequence, the maximum meniscus height was averaged on the basis of over a several high-speed camera photos. It was also observed that the numerical results were within the standard deviation interval of the experiment for low and medium induction power, i.e. Variant 1 and 2, respectively. For the highest induction power (Variant 3), the numerical meniscus height was 0.231 m. In this case, the numerical results were not within the standard deviation limits. However, the relative error was still low and amounted to approximately 4%. This could be the result of high

instabilities in the free surface, making the measurement reading difficult.

The influence of the inductor power on the meniscus shape was crucial. For higher power values, the free surface of the molten metal was significantly larger, and its shape became flatter. The absolute difference between the successive variants was 0.015 m. Moreover, for the lowest input power, the location of the contact point of the meniscus and the crucible was the highest. Therefore, by decreasing the inductor power, the contact area of the molten metal and crucible could be limited. This observation is crucial for the impurity removal process.

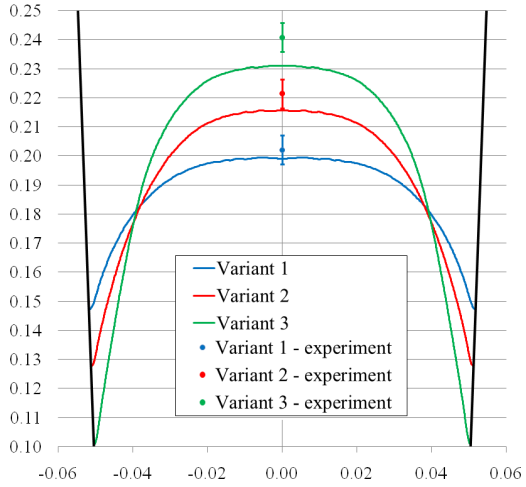

Figure 2 Numerical and experimental results of the meniscus shape (in m) for different inductor powers.

Once the meniscus was formed, the purification process was analysed. The computations for the real time of 30 min were performed. The initial value of the lead mass fraction in the charge was of 2%. In addition, a uniform distribution of this inclusion was assumed. The smallest area and the highest averaged lead mass fraction were observed for Variant 1, which is characterised by the smallest input power. With the increase of inductor power, the meniscus area increased and the averaged lead mass fraction decreased. For Variant 3, over 40% of the initial lead mass was removed from the charge. In addition, the mass fraction of lead was uniformly distributed showing a difference between lowest and highest value of approx. 0.01 %. The highest concentration of lead was observed for the lower region of the charge. An area near the free surface was characterised by the lead lower mass fraction. The lead distribution is strongly combined with the vortices which were formed within the molten metal.

CONCLUSION

A numerical model of a vacuum induction furnace with a two-way coupling procedure was proposed. To reduce the computing time, only a single segment of the whole 3-D domain was analysed. The data transfer between the EMAG and CFD submodels was developed to ensure effective time marching. The investigation was performed for different inductor coil input power.

The comparison between the numerical results and the experimental data showed a very good agreement in terms of the free surface modelling. The meniscus for two of the three studied cases was predicted within the measurement accuracy. The relative error between the numerical and experimental data for every tested variant was lower than 4%.

The purification process of copper-lead alloy was examined for three inductor power values. It was observed that influence of induction furnace power was crucial for the meniscus formation. Moreover, for higher input power the intensity of purification process is higher because the area of free surface directly corresponds to the mass transport through the interface.

REFERENCES

[1] Yang J., Chen R., Ding H., Guo J., Han J. and Fu H., Thermal characteristics of induction heating in cold crucible used for directional solidification, *Applied Thermal Engineering*, Vol. 59, 2013, pp. 69-76

[2] Hadad Y., Kochavi E. and Levy A., Inductive heating with a stepped diameter crucible, *Applied Thermal Engineering*, Vol. 102, 2016, pp. 149-157

[3] Bojarevics V., Harding R.A., Pericleous K. and Wickins M., The development and experimental validation of a numerical model of an induction skull melting furnace, *Metallurgical and Materials Transactions, B*, Vol. 35B, 2004, pp. 785-803

[4] Spitans, S., Jakovics, A., Baake, E. and Nacke, B., Numerical modelling of free surface dynamics of conductive melt in the induction furnace, *Magnetohydrodynamics*, Vol. 46, 2010, pp. 317-328

[5] Song, J.H., Min, B.T., Kim, J.H., Kim, H.W., Hong, S.W. and Chung, S.H., An electromagnetic and thermal analysis of a cold crucible melting, *International Communications in Heat and Mass Transfer*, Vol. 32, 2005, pp. 1325-1336

[6] Liu, T., Dong, Z., Zhao, Y., Wang, J., Chen, T., Xie, H., Li, J., Ni, H. and Huo, D., Purification of metallurgical silicon through directional solidification in a large cold crucible, *Journal of Crystal Growth*, Vol. 355, 2012, pp. 145-150

[7] Buliński, P., Smołka, J., Golak, S., Przyłucki, R., Blacha, L., Białecki, R., Palacz, M. and Siwiec, G., Effect of turbulence modeling in numerical analysis of melting process in an induction furnace, *Archives of Metallurgy and Materials*, Vol. 60, 2015, pp. 1575-1579

[8] Buliński, P., Smołka, J., Golak, S. and Przyłucki, R., Coupled numerical model of metal melting in an induction furnace: sensitivity analysis and validation of model, *Przeglad elektrotechniczny*, Vol. 92, 2016, pp. 49-52

[9] Buliński, P., Smołka, J., Golak, S., Przyłucki, R., Palacz, M., Siwiec, G., Lipart, J., Białecki, R. and Blacha, L., Numerical and experimental investigation of heat transfer process in electromagnetically driven flow within a vacuum induction furnace, *Applied Thermal Engineering*, (under review)

[10] Umbrasko, A., Baake, E., Nacke, B. and Jakovics, A., Numerical studies of the melting process in the induction furnace with cold crucible, *Proceedings of HES-07 conference*, Padova, Italy, Paper: 277-292, 2007

[11] Pericleous K., Bojarevics V., Djambazov G., Harding R.A. and Wickins M., Experimental and numerical study of the cold crucible melting process, *Applied Mathematical Modelling*, Vol. 30, 2006, pp. 1262-1280